Type B aortic dissection in Marfan patients after the David procedure: Insights from patient-specific simulation

Farshad Tajeddini, MASc,[a] David A. Romero, PhD,[a] Yu Xuan Huang,[b] Tirone E. David, MD,[c] Maral Ouzounian, MD, PhD,[c] Cristina H. Amon, ScD,[a,d] and Jennifer C. Y. Chung, MD, MSc[c,d]

ABSTRACT

Objective: An elevated risk of acute type B aortic dissection exists in patients with Marfan syndrome after the David procedure. This study explores hemodynamic changes in the descending aorta postsurgery.

Methods: A single-center retrospective review identified 5 patients with Marfan syndrome who experienced acute type B aortic dissection within 6 years after the David procedure, alongside 5 matched patients with Marfan syndrome without dissection more than 6 years postsurgery. Baseline and postoperative computed tomography and magnetic resonance scans were analyzed for aortic geometry reconstruction. Computational fluid dynamic simulations evaluated preoperative and postoperative hemodynamics.

Results: Patients with acute type B aortic dissection showed lower blood flow velocities, increased vortices, and altered velocity profiles in the proximal descending aorta compared with controls. Preoperatively, median time-averaged wall shear stress in the descending aorta was lower in patients with acute type B aortic dissection (control: 1.76 [1.50-2.83] Pa, dissection: 1.16 [1.06-1.30] Pa, $P = .047$). Postsurgery, neither group had significant time-averaged wall shear stress changes (dissection: $P = .69$, control: $P = .53$). Localized analysis revealed surgery-induced time-averaged wall shear stress increases near the subclavian artery in the dissection group (range, +0.30 to +1.05 Pa, each comparison, $P < .05$). No such changes were observed in controls. Oscillatory shear index and relative residence time were higher in patients with acute type B aortic dissection before and after surgery versus controls.

Conclusions: Hemodynamics likely play a role in post–David procedure acute type B aortic dissection. Further investigation into aortic geometry, hemodynamics, and postoperative acute type B aortic dissection is vital for enhancing outcomes and refining surgical strategies in patients with Marfan syndrome. (JTCVS Open 2024;21:1-16)

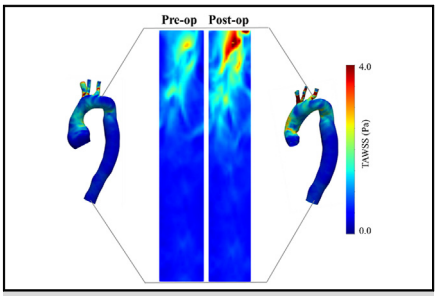

Preoperative and postoperative TAWSS of patients with MFS with post-VSRR type B aortic dissection.

CENTRAL MESSAGE

Patient-specific simulations and hemodynamic analysis reveal that both anatomic and surgically induced geometric features in patients with MFS may play a role in post-VSRR type B aortic dissection.

PERSPECTIVE

Since the introduction of the David procedure, patients with MFS have experienced improved lives with reduced risks of type A aortic dissection and valve-related complications. However, there is an elevated rate of postrepair ATBADs. Computational simulations can provide insight into the complex interplay among patient anatomy, hemodynamics, and ATBAD.

See Discussion on page 17.

From the Departments of [a]Mechanical & Industrial Engineering and [b]Engineering Science, [c]Division of Cardiovascular Surgery, University Health Network, and [d]Institute of Biomedical Engineering, University of Toronto, Toronto, Ontario, Canada.

The study received approval from the Toronto General Hospital (Research Ethics Board No: 21-5858.3, November 17, 2021). Consent was waived because of the retrospective analysis of imaging from patients involved.

Peter Munk Cardiac Center Innovation Fund (No. 5790-5090-0602). Natural Sciences and Engineering Research Council of Canada (Funder ID: 10.13039/501100000038).

Read at the 104th Annual Meeting of The American Association for Thoracic Surgery, Toronto, Ontario, Canada, April 27-30, 2024.

Received for publication Feb 11, 2024; revisions received April 3, 2024; accepted for publication April 17, 2024; available ahead of print May 16, 2024.

Address for reprints: Jennifer C. Y. Chung, MD, MSc, Division of Cardiovascular Surgery, University Health Network, University of Toronto, Toronto, Ontario, Canada M5G 2C4 (E-mail: jennifer.chung@uhn.ca).

2666-2736

https://doi.org/10.1016/j.xjon.2024.04.017

Abbreviations and Acronyms

ATBAD = acute type B aortic dissection
BC = boundary condition
CFD = computational fluid dynamics
4D = 4-dimensional
MFS = Marfan syndrome
MRI = magnetic resonance imaging
OSI = oscillatory shear index
pDTA = proximal descending thoracic aorta
RRT = relative residence time
TAWSS = time-averaged wall shear stress
VSRR = valve-sparing root replacement
WSS = wall shear stress

To view the AATS Annual Meeting Webcast, see the URL next to the webcast thumbnail.

Aortic root aneurysms represent the primary cause of morbidity and mortality in patients with Marfan syndrome (MFS).[1] The David procedure, introduced in 1992 specifically for those with MFS, is an aortic valve-sparing root replacement (VSRR) technique that eliminates the risk of type A aortic dissection and offers exceptional long-term freedom from aortic valve reoperation or insufficiency.[2,3] However, we and others reported a 20-year acute type B aortic dissection (ATBAD) rate of 19% to 20% after proximal repair for patients with MFS.[3,4]

Type B dissections typically occur in aortas with relatively normal dimensions, making them challenging to predict. This elevated rate of ATBAD may be related to intrinsic weakened aortic tissue properties related to MFS or pathological hemodynamic forces, such as altered wall shear stress (WSS), which in turn are correlated with mechanical properties of the aortic wall.[5,6] Evidence suggests that hemodynamic indices vary between patients with MFS and patients without MFS.[6-9] The diverse aortic anatomy among patients with MFS and the alterations in aortic geometry induced by the David procedure can collectively influence postoperative blood flow patterns and WSS. These factors may contribute to future complications, including ATBAD.

Thus, it appears imperative to quantify WSS to better understand hemodynamic risk factors for ATBAD. In this regard, 4-dimensional (4D) magnetic resonance imaging (MRI) and computational fluid dynamics (CFD) provide noninvasive insights into blood velocity, streamlines, and WSS within the cardiovascular system.[8,9] However, the limited spatiotemporal resolution of 4D MRI, along with noise-related phase errors, adversely affects the accuracy of its results.[10] In contrast, patient-specific CFD simulations offer superior spatial and temporal resolution compared with 4D MRI.[11] With the use of CFD, Nannini and colleagues[12] recently showed that implanting a graft induces changes in the hemodynamics and biomechanics in the thoracic aorta, potentially initiating adverse vessel remodeling. Wang and colleagues[6] indicated that although anatomic features remain critical for assessing the risk of ATBAD development, hemodynamic analyses have shown promising potential.

Therefore, we aim to conduct a CFD comparison between patients with MFS who developed post-VSRR ATBAD and patients who did not to determine hemodynamic differences based on their baseline aortic geometry. Additionally, we aim to explore the influence of the VSRR itself in altering hemodynamics in the descending thoracic aorta. By conducting both comparisons, we tease out whether ATBAD may be predictable in patients with MFS based on hemodynamics and how we conduct the original VSRR plays a role in influencing this risk.

MATERIALS AND METHODS

Image Acquisition

A retrospective study was designed by assessing the medical records of patients with MFS who underwent the David procedure at Toronto General Hospital. Of 203 patients with MFS, 5 had distal aortic dissections after VSRR (dissection group). We selected another 5 patients from the original cohort, matched for age and gender to the patients in the dissection group, who also underwent VSRR but did not develop distal dissections after at least 6 years of follow-up (control group). For both groups, we gathered prerepair, postrepair, and follow-up computed tomography or MRI scans (scan resolution varying between 0.6 and 3.0 mm), including post-ATBAD if applicable.

Patient-Specific Computational Modeling

Figure 1 depicts the computational methodology used in this study. We previously published our workflow to reconstruct aortic geometries using ITK-SNAP.[13-15] Subsequently, the reconstructed geometry is adjusted to prepare it for numerical flow simulations. More specifically, surface smoothing operations are implemented in MeshMixer ([RRID:SCR_015736] AM) to reduce reconstruction noise caused by measurement variations in the computed tomography/MRI images. Significant effort was made to ensure that the level of smoothness did not lead to simplification of the geometry or the exclusion of any geometric features. Following a mesh study on parameters of interest, 2,500,000 elements (element size = 1e-3) were chosen for this study.

The governing equations are the continuity and the Navier-Stokes equations. Transient, laminar, Newtonian, and incompressible flow simulations in ANSYS were conducted for 4 cardiac cycles to ensure that the results converged to steady-periodic flows, but only the fourth cycle was used for the postprocessing of the results. The viscosity and density parameters were set to $\mu = 0.004$ Pa·s and $\rho = 1060$ kg·m̂–3, respectively.[13] The vessel wall was assumed to be rigid. For the inlet boundary condition (BC), a generic time-varying waveform derived from averaging the flow waveforms of 40 patients with accessible 4D MRI scans was used.[16] The waveform was scaled based on anthropometric data of patients to match their cardiac output and was applied to all patients.[17,18] For the outlet BC, a 3-element Windkessel model was used to include the resistance of the downstream vasculature.[19]

Postsimulation, the 90th percentile WSS, time-averaged wall shear stress (TAWSS), oscillatory shear index (OSI), and relative residence

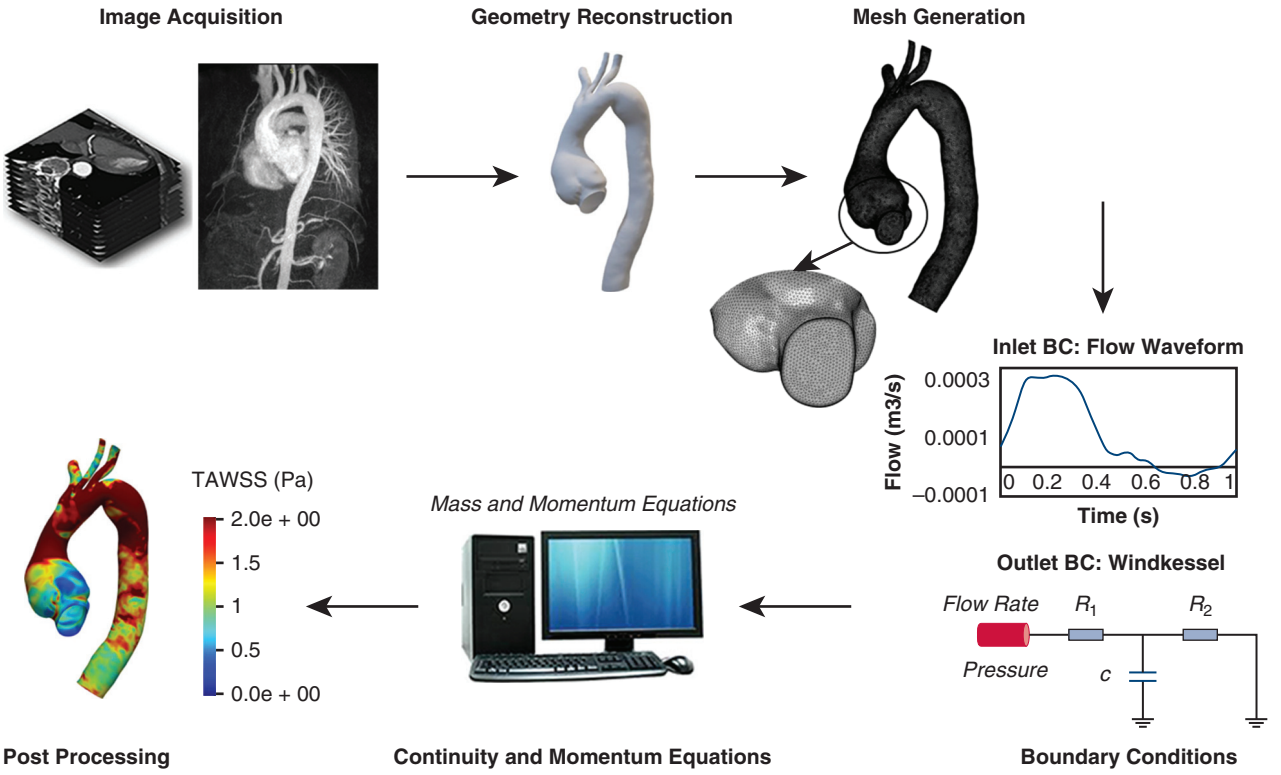

FIGURE 1. Schematic of the computational workflow used in this study. *BC*, Boundary condition; *TAWSS*, time-averaged wall shear stress.

time (RRT) were assessed both globally across the entire descending aorta and locally within different segments of the descending aorta.

Statistical Analysis

Statistical analysis was conducted using an in-house Python code. Hemodynamic parameters were analyzed for the dissection and control groups preoperatively and postoperatively. The Kolmogorov-Smirnov test assessed the normality of the distribution. For normally distributed data, a Student *t* test was used, and the Mann–Whitney *U* test was used for non-normally distributed data.

RESULTS

Patient Demographics

Patient demographics are summarized in Table 1. The dissection group consisted of 5 patients aged 37 ± 13 years at the time of the original VSRR. The median of time from surgery to occurrence of the ATBAD was 3 years (range, 0.8-6 years). The control group consisted of 5 patients aged 32 ± 13 years at the time of the original VSRR, and their median length of follow-up without ATBAD was 6.2 years (6-7 years).

For the matching process, our focus was on age and sex. Sex plays a crucial role in estimating cardiac output due to differing assumptions for men and women. Additionally, our prior study demonstrated that the spatial distribution of the inlet BC minimally impacts hemodynamic parameters in the descending aorta.[14] Thus, scaling the inlet BC by patients' cardiac output sufficed for evaluating hemodynamic parameters in this region, aligning with findings in other studies for type B aortic dissection.[20] Toward this end, we used patients' heights and weights to derive their body surface area, which was then used to calculate cardiac output for adjusting our inlet BC accordingly.[17,18] Moreover, age was prioritized for matching because of its significant influence as the strongest predictor of material properties of the aortic wall.[21]

Streamline

A qualitative analysis was conducted of the blood flow streamlines and their velocities throughout the cardiac cycle. We focused on the proximal descending thoracic aorta (pDTA), the site most prone to primary intimal tears. We observed consistent patterns across pairs, and pair 1 is detailed as an illustration in Figure 2.

During flow acceleration, the streamlines are well organized for both patient groups, and small vortices can be observed near the valve preoperatively. As one moves distally along the aorta, areas of maximal velocity, whether along the inner or outer curvatures of the aorta, changes. The preoperative and postoperative difference between this eccentricity of velocity profiles is more pronounced in patients in the dissection group, whereas for control patients, the velocity contours remained similar.

During peak systole, velocity increases, and vortices near the valve become stronger, causing disruption in the

TABLE 1. Patient demographics

Patient pair	Group	Age, y	Gender	Height (cm)	Weight (kg)	Preoperative AI	Postoperative AI	Preoperative EF (%)	Postoperative EF (%)	Concomitant procedures
Pair 1	Dissection	60	F	182	88	Mild to moderate AI	Mild AI	60	40	-
	Control	50	F	185	79	Mild to moderate AI	Trace AI	60	49	-
Pair 2	Dissection	36	M	185	91	Mild to moderate AI	Trace AI	60	60	-
	Control	32	M	180	58	Trace AI	Trace AI	60	60	
Pair 3	Dissection	37	M	188	86	Moderate AI	Trace AI	60	60	-
	Control	39	M	200	97	Trace AI	No AI	60	60	Redo sternotomy, Mitral valve repair
Pair 4	Dissection	51	M	185	70	Mild AI	Mild AI	60	60	-
	Control	54	M	185	77	Severe AI	Trace AI	60	50	CABG
Pair 5	Dissection	27	M	174	82	Mild to moderate AI	Trivial AI	60	60	-
	Control	25	M	196	73.5	No AI	No AI	55	40	-

AI, Aortic insufficiency; *EF*, ejection fraction; *CABG*, coronary artery bypass grafting.

streamlines for both patients and generating a helical motion. This helical motion is a result of the secondary flow superimposed onto the main flow of the sweeping jet. Therefore, a region of high velocity magnitude originating from the jet is carried along the aortic arch. Subsequently, a high-momentum flow propagates into the pDTA. This disturbs the eccentricity of velocity profiles, causing the region of high velocities to get closer to the outer curvature compared with the previous timepoint. Near the inner curvature, although there are still regions of lower velocity, regions of high velocity also appeared. Once again, the differences in preoperative and postoperative velocity contours are more pronounced for patients with dissection compared with the control group.

During flow deceleration, a stronger recirculating zone is observed for both patient groups, leading to more disorganized streamlines potentially due to the instability caused by the flow deceleration. For patients in the dissection group, vortices are present near both the inner and outer curvatures of the pDTA, and they are stronger and have higher momentum after the operation. In contrast, for control patients, this disturbed flow is shaped slightly further distal to the subclavian artery with weaker vortices. Additionally, after the operation, these vortices tend to be closer to the centerline of the vessel rather than the wall. In terms of velocity profiles, for the dissection group, both preoperatively and postoperatively, a low velocity magnitude immediately downstream of the subclavian artery is seen. However, an increase in velocity is then observed, near the inner curvature especially and the outer curve, indicating the presence of vortices. On the other hand, for the control group, profiles and their eccentricity are consistent across the proximal descending aorta, and the velocity levels are lower than in the dissection group, unlike at the previous time points. This suggests that control patients exhibit more stable flow in the pDTA compared with patients with dissection. The same results can be seen for reverse flow and diastole time points.

Velocity Vectors

Figure 2 provides a visual representation the velocity vectors for pair 1 preoperatively and postoperatively. Notably, when examining patients in the dissection group, the differences between preoperative and postoperative conditions are more pronounced compared with control patients. For instance, during the flow acceleration phase, there is observable flow separation in the pDTA postsurgery, leading to a noticeable alteration in the velocity vector compared with the preoperative condition. Conversely, for the same timepoint, when compared with control patients, there is a similar pattern in velocity vectors in preoperative and postoperative stages. Another significant observation is that postsurgery, velocity vectors in the dissection group shift orthogonal to the outer curvature of the pDTA, whereas in the control patients, they reduce, disappear, or shift downstream.

Wall Shear Stress

An analysis was performed on the WSS throughout the cardiac cycle. We observed consistent patterns across pairs. Figure 3, *A* presents a 3-dimensional contour of WSS at different time points throughout the cardiac cycle. Generally, the level of WSS is lower for patients with dissection compared with the control group, both before

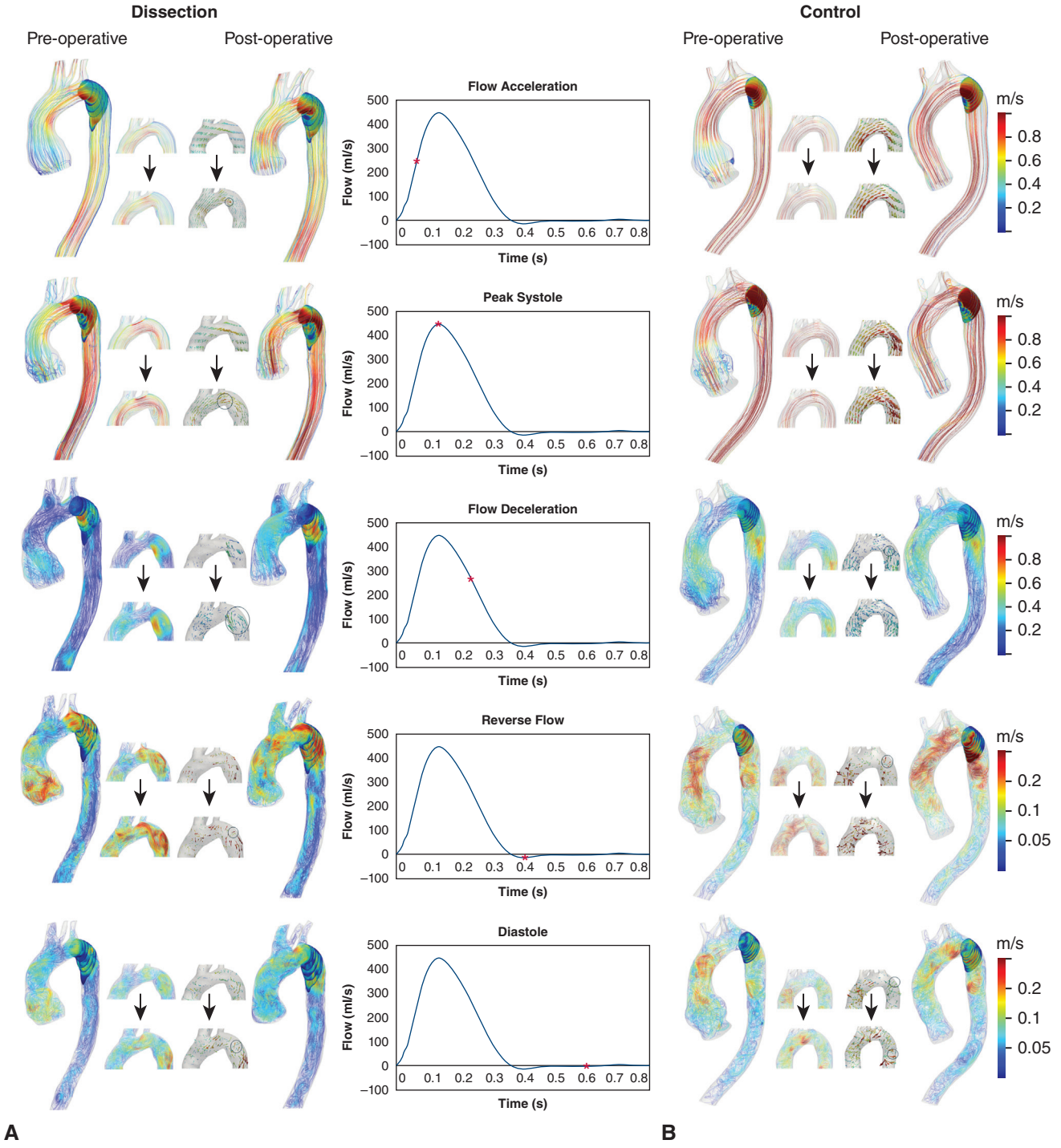

FIGURE 2. Preoperative and postoperative streamlines colored by velocity magnitude, along with velocity profiles and velocity vectors in the proximal section of the descending aorta for (A) patient with dissection and (B) control patient of pair 1 at various timepoints over a cardiac cycle.

and after the operation. Moreover, during flow acceleration, peak systole, and flow deceleration, the dissection group shows a significant increase ($P < .05$) in circumferentially median WSS postoperatively at the pDTA, whereas for control patients, there is an insignificant or a significant decrease ($P < .05$) in circumferentially median WSS after the operation in the same location (Figure 3, *B*). However, during reverse flow and diastole, both patient groups show a significant increase in WSS after the operation.

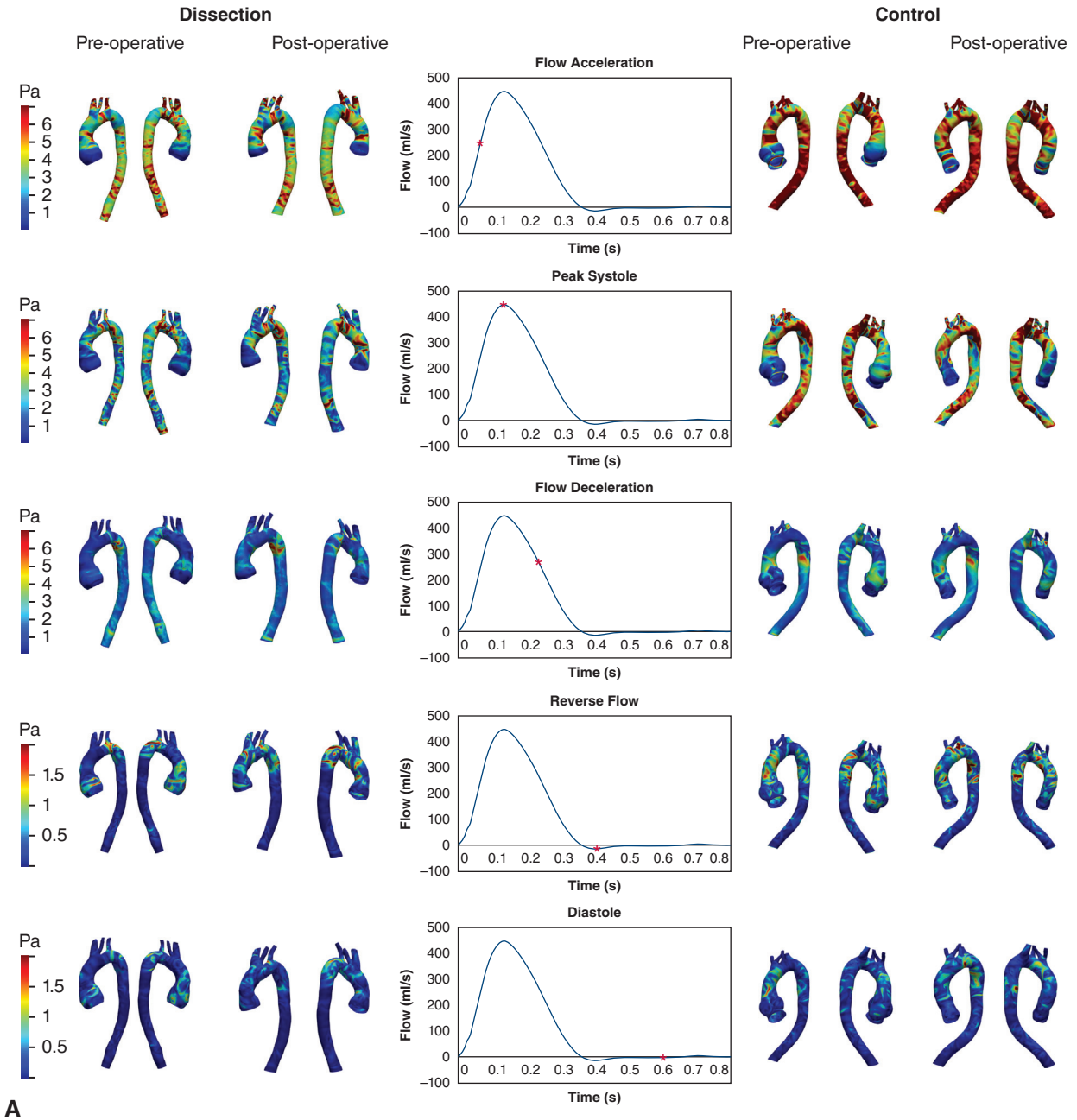

FIGURE 3. A, Preoperative and postoperative WSS at various timepoints over a cardiac cycle. B, Preoperative and postoperative median of TAWSS along the length of the descending aorta at peak systole for pair 1 displays the curve of medians for different segments of the descending aorta starting from the subclavian artery. The curves show that the postoperative medians near the subclavian artery exhibit a significant increase ($P < .05$, largest ratio of post/pre = 1.4) for the patient with dissection, whereas the same change is not observed for the control patient, and the differences are insignificant in the same section ($P > .05$).

Time-Averaged Wall Shear Stress

Figure 4 depicts TAWSS analysis for pair 1, with results of the rest of the cohort provided in the Supplementary material (Figures E1-E4). The patients who experienced ATBAD during the follow-up period exhibited a lower median TAWSS in the descending aorta when compared with the control group at baseline (control: 1.76 [1.50-2.83] Pa, dissection: 1.16 [1.06-1.30] Pa, $P = .047$) (Figure 5, *A*). On examination of the effect of surgery, neither the dissection group ($P = .69$) nor the control group ($P = .53$) exhibited statistically significant changes in median TAWSS after surgery. However, on closer examination through localized analysis, which can be seen in Figure 4 for pair 1 and Figure 6 for all pairs, the David procedure resulted in a focal increase in TAWSS ranging from +0.30 Pa to +1.05 Pa (each comparison, $P < .05$) near the subclavian artery for the dissection group. In contrast, this was not observed for the control group.

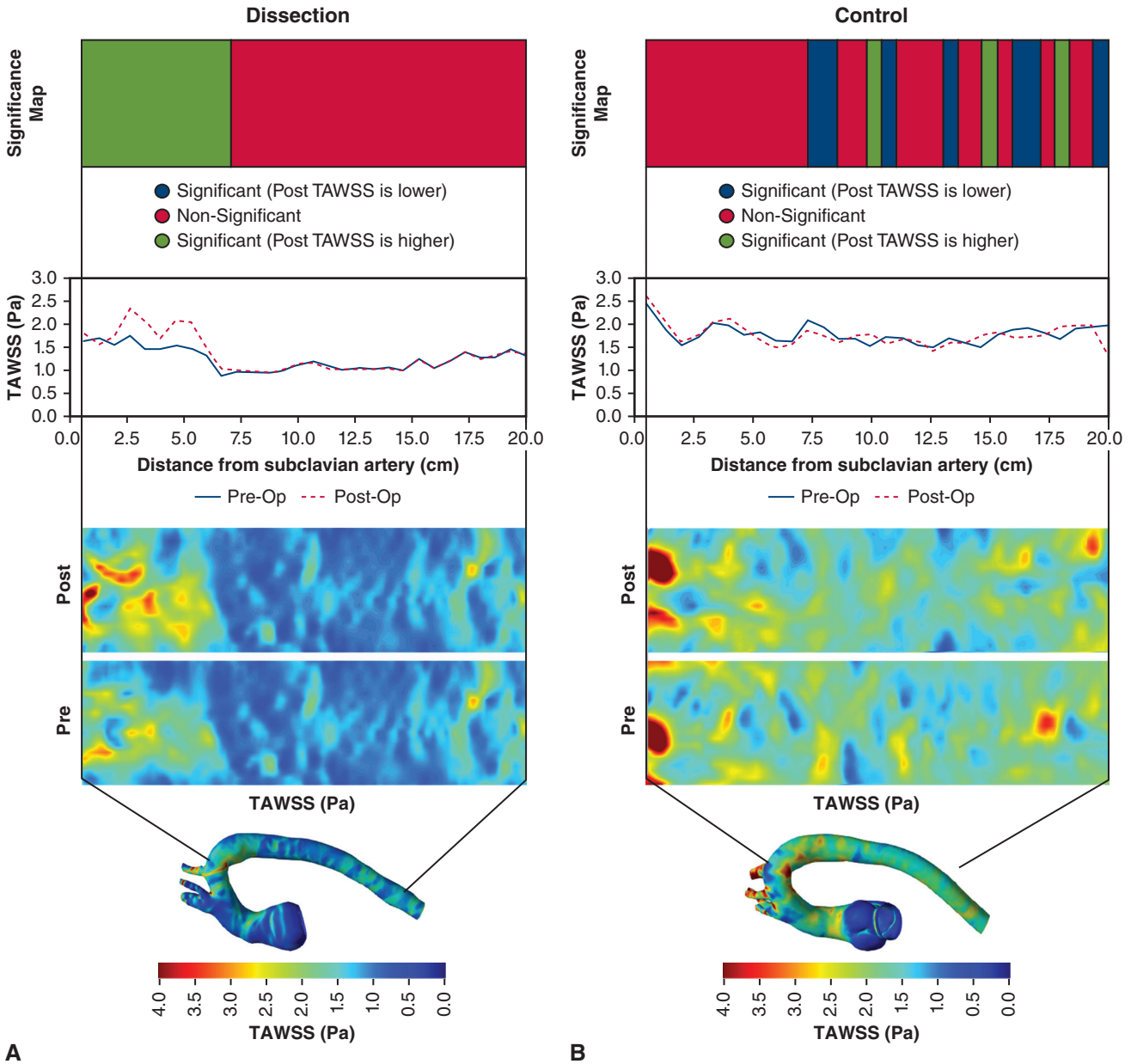

FIGURE 4. Comprehensive analysis for the first pair, comprising a preoperative 3-dimensional contour of TAWSS on the thoracic aorta, preoperative and postoperative 2-dimensional maps of TAWSS, a curve illustrating the preoperative and postoperative medians over different segments of the descending aorta, and a map displaying the *t* test results for differences in postoperative and preoperative TAWSS for each segment. In the *t* test map, *green* indicates a significant increase in TAWSS after the operation, *blue* indicates a significant decrease, and *red* denotes no significant difference in preoperative and postoperative TAWSS. Also, each segment represents a 5-mm interval. *TAWSS*, Time-averaged wall shear stress

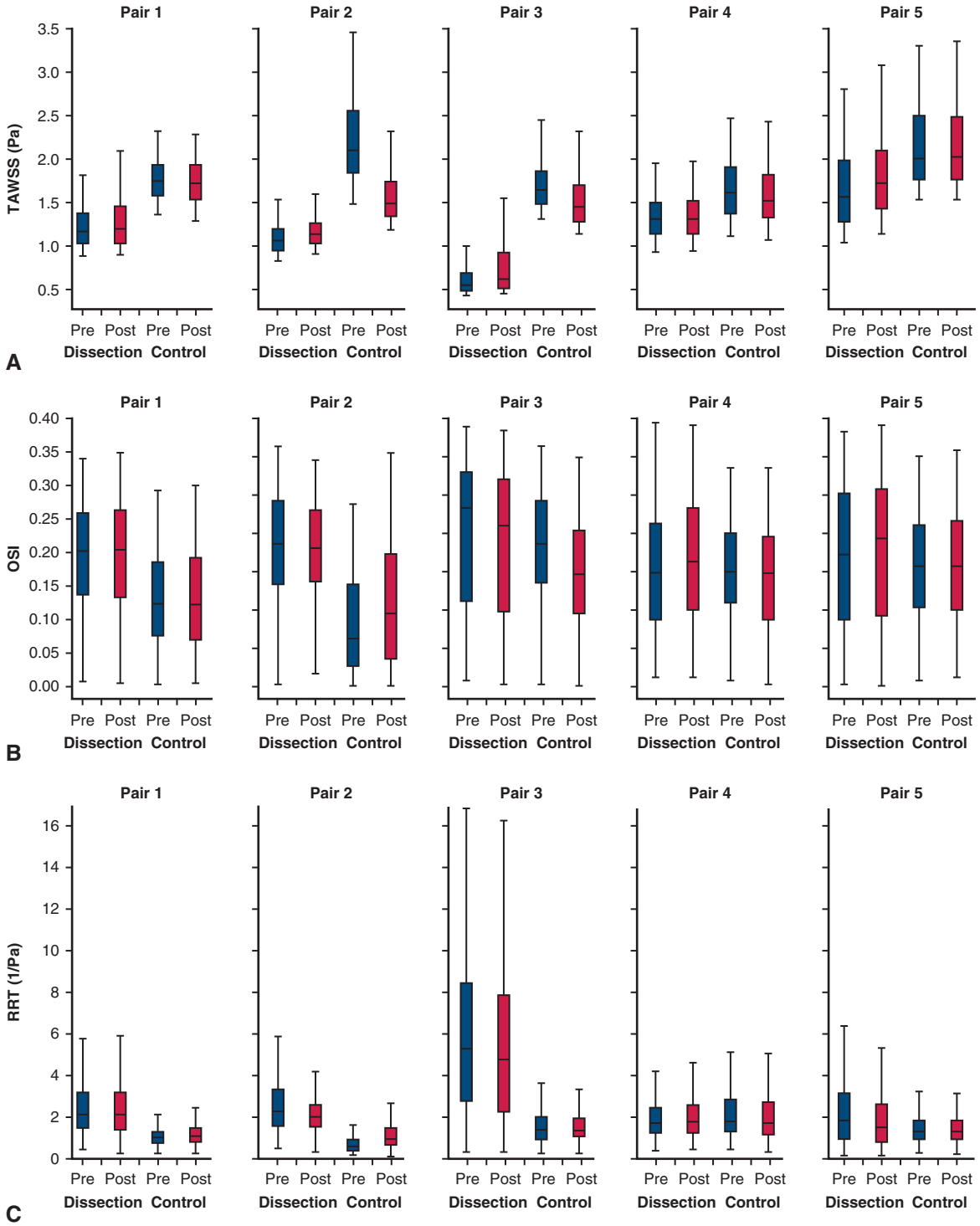

FIGURE 5. Box plots of preoperative and postoperative (A) TAWSS, (B) OSI, and (C) RRT for patients with dissection and control patients. The lower and upper borders of the box represent the lower and upper quartiles (25th percentile and 75th percentile). The middle horizontal line represents the median. The lower and upper whiskers represent the minimum and maximum values of nonoutliers. *RRT*, Relative residence time; *OSI*, oscillatory shear index; *TAWSS*, time-averaged wall shear stress.

Oscillatory Shear Index

An examination of patients who experienced ATBAD during the follow-up period showed a nonsignificant higher median OSI in the descending aorta compared with the control group at baseline (control: 0.13 [0.08-0.18] Pa, dissection: 0.20 [0.18-0.21] Pa, $P = .11$) (Figure 5, *B*). Analyzing

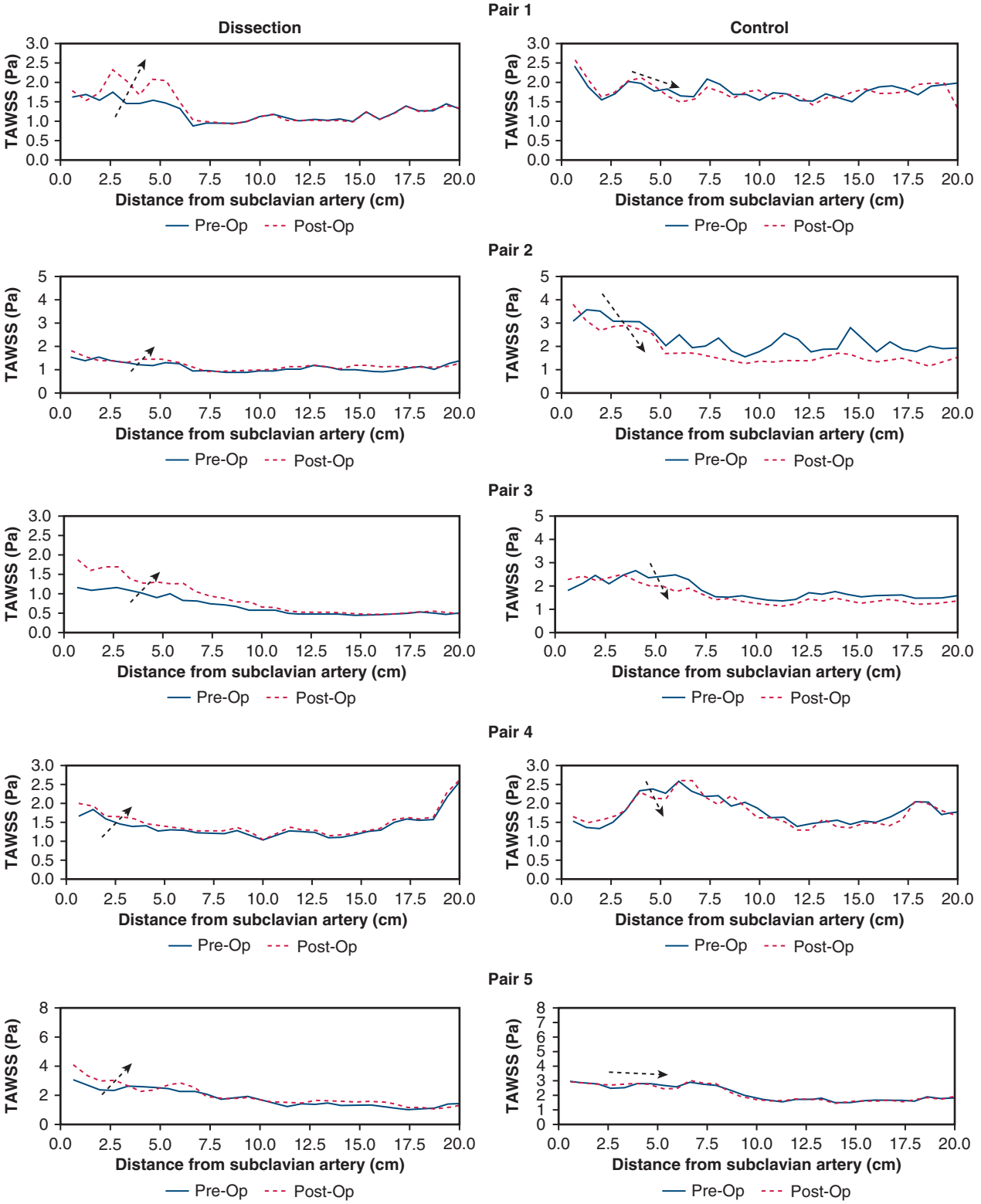

FIGURE 6. Curve of median TAWSS across different segments of the descending aorta, starting from the subclavian artery. *TAWSS*, Time-averaged wall shear stress.

the impact of surgery (postoperative OSI) revealed a significant difference in OSI between the control and dissection groups (control: 0.13 [0.11-0.17], dissection: 0.21 [0.20-0.21], $P = .02$). Additionally, a detailed examination of localized OSI between preoperative and postoperative for the control or dissection groups did not reveal any specific trend.

Relative Residence Time

Patients who had ATBAD after VSRR showed elevated levels of RRT compared with those without ATBAD both before and after surgery (Figure 5, *C*). There was no statistically significant difference between pre- and post-VSRR medians RRT in the control group ($P = .819$) and dissection group ($P = .69$). Comparing preoperative and postoperative medians RRTs for the dissection and control groups indicates a significant difference in RRT both preoperatively (control: 1.15 [0.68-1.39] 1/Pa, dissection: 2.15 [1.85-2.23] 1/Pa, $P = .017$) and postoperatively (control: 1.18 [0.98-1.36] Pa, dissection: 1.99 [1.54-2.10] 1/Pa, $P = .015$).

DISCUSSION

CFD models of the aorta can be used to explore the hemodynamic underpinnings of the elevated rates of ATBAD after VSRR in the population with MFS. Our study uncovered notable differences in blood flow dynamics between patients who experienced ATBAD and control subjects both before and after VSRR. Specifically, patients with dissection exhibited consistently lower blood flow velocities in the descending aorta compared with control patients, a pattern observed both pre- and post-VSRR. Furthermore, post-VSRR, patients who go on to dissect displayed increased vortices in the pDTA and altered eccentricity of the velocity profile, particularly toward the outer curvature wall. This postoperative alteration in flow dynamics was distinct not only from the preoperative condition but also compared with control subjects. Additionally, WSS across the descending aorta was lower in patients who go on to develop ATBAD compared with controls. However, after VSRR, patients with dissection exhibited a significant focal increase in TAWSS, contrasting with a significant decrease or no significant change in TAWSS observed in control subjects (Figure 7). Moreover, levels of OSI and RRT were consistently higher in the dissection groups compared with control groups, both preoperatively and postoperatively.

These results add to the growing literature supporting at least a partially hemodynamic pathophysiology for the development of ATBAD in this population. A 4D MRI study performed in 24 patients with MFS and 10 volunteers highlighted the presence of significant flow alterations, including enhanced vortex flow in the pDTA, in patients with MFS compared with healthy volunteers.[22] Additionally, similar to our study, the study underscores the importance of hemodynamics in the pDTA because it is a

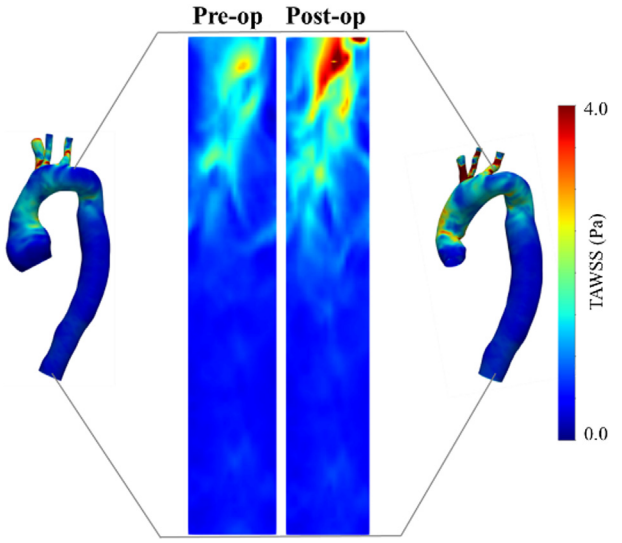

FIGURE 7. Preoperative and postoperative TAWSS of patients with MFS with post-VSRR type B aortic dissection.

frequent site of the primary intimal tear. In another study involving 12 patients with MFS who underwent root replacement, findings revealed abnormal flow patterns and decreased WSS in 1 patient who subsequently developed ATBAD.[23] Other 4D flow cardiovascular magnetic resonance study on 19 patients with MFS and 10 volunteers exhibited reduced segmental WSS in the inner pDTA, which corresponds to heightened localized abnormal vortex/helix flow patterns and an enlarged diameter at a key site associated with ATBAD.[24] Moreover, another 4D cardiovascular magnetic resonance study on 25 patients with MFS and 21 healthy controls showed that in children and young adults with MFS, notable changes in aortic flow patterns and a decrease in WSS are evident in the proximal ascending thoracic aorta and pDTA, again segments commonly associated with the initiation of aortic dissection.[9] In addition, a 4D cardiovascular magnetic resonance study on 75 patients with MFS and 48 healthy subjects showed that patients with MFS, including those without aortic dilation, exhibited reduced in-plane rotational flow and circumferential WSS in both the distal ascending thoracic aorta and the pDTA.[8]

Near wall hemodynamics such as WSS has a biological impact on the adjacent tissue. The combination of lower TAWSS and higher OSI in the dissection group results in greater shear reversal, which is associated with endothelial dysfunction. This dysfunction might be related to the infiltration of particles into the arterial wall, a phenomenon previously observed in coronary arteries.[25,26] The elevated RRT that we observed for patients in the dissection group is potentially associated with the infiltration of plasminogen activators into the arterial wall, because RRT measures the duration particles remain adjacent to the wall. These activators might interact with smooth muscle cells, damaging the

extracellular matrix.[27-29] We hypothesize that over time, this weakens the aortic wall, rendering it more prone to dissection.

Furthermore, we hypothesize that the postoperative flow impingement in the pDTA that we see in the dissection group, along with the redirection of velocity vectors predominantly orthogonal rather than parallel to the outer curvature, could potentially exert unwanted additional force on the weakened aortic wall, leading to a sudden-onset primary intimal tear. Future studies are required to evaluate the accuracy of these hypotheses.

Other future work will also concentrate on whether we may predict, by baseline anatomy or influence through surgical repair, hemodynamic parameters in the descending thoracic aorta. Because velocity is influenced by geometric features, such as diameter of ascending thoracic aorta, arch and pDTA, jet flow impingement, flow separation due to surgically induced kinks, and so forth, and WSS is derived from the velocity field, it is logical to link the lower levels of WSS to the geometric features of the thoracic aorta. Both anatomic geometric features and surgically induced factors appear to contribute to disturbed flow patterns and hemodynamic variations that may play a role in the onset of ATBAD. This is because the analysis of baseline conditions reveals a significant difference between dissection and control groups for TAWSS and RRT, primarily due to anatomic geometric features. However, OSI shows insignificant differences between control and dissection groups at baseline, with significance emerging postoperation, indicating the influence of surgery. Furthermore, segmental analysis of the descending aorta demonstrates a significant increase in TAWSS in the pDTA for patients with dissection postsurgery compared with preoperative levels, whereas for control patients, it remains insignificant or exhibits a significant decrease.

In terms of the clinical implications of this study, our initial focus would be to discover the anatomic geometric factors responsible for variations in hemodynamic parameters between the dissection and control groups through using concepts such as statistical shape analysis and principal component analysis. These concepts have been used in multiple articles in the literature.[30,31] Subsequently, by exploring the impact of key geometric alterations induced by the David procedure on distal aortic hemodynamics, we can then use statistical tools to manipulate these factors within a defined range. We will create a virtual surgical repair method and its associated simulation tool for the David procedure, encompassing various repair strategies while considering significant geometric features. This tool will analyze graft configurations based on a patient's pre- and postrepair hemodynamics to identify, from a hemodynamics standpoint, the most favorable personalized repair approach, with the aim of reducing the risk of type B aortic dissection in patients with MFS post-VSRR.

Study Limitations

A major limitation of this study is the relatively small sample size primarily due to variability in scan resolution and the availability of patient scans at different time points (preoperation, postoperation, and postdissection). The retrospective nature of this study with a limited number of patients with complete imaging data made it impossible to fully control for all pertinent confounding variables. However, it is important to acknowledge that the dataset we used is one of the richest available for patients with MFS, comprising 203 individuals, which formed the basis of this retrospective study. Another limitation applies to the assumption of a constant inlet flow rate for all patients in both preoperative and postoperative conditions, despite potential differences in individual cardiac output that could impact the analysis. However, this approach allowed us to isolate the influence of geometric features on hemodynamics, which was the primary focus of this article. Also, in our recently published study,[13] we showed that hemodynamic parameters are less sensitive to the type of inlet BC in the descending aorta. Additionally, the assumption of rigid walls may be considered a limitation. In reality, the material properties of the graft differ from those of the aortic wall, potentially influencing the pulse wave velocity of the jet impacting the ascending aorta and propagating to the arch and descending aorta.[12] Nonetheless, even under the assumption of rigid walls, we were able to predict differences in flow distribution in the proximal section of the descending aorta between patients with dissection and control patients. We anticipate further insights from fluid-structure interaction simulations, which are part of our ongoing study. Moreover, patients with MFS typically exhibit greater wall rigidity compared with healthy individuals.[32] Given the number of publications on thoracic aorta of healthy individuals under rigid assumption,[33,34] considering rigid assumption for patients with MFS may be acceptable.

CONCLUSIONS

The development of ATBAD in patients with MFS post-VSRR was associated with a significantly lower median TAWSS and higher OSI and RRT at baseline. Moreover, the alteration of geometric characteristics in the ascending aorta through the David procedure led to a localized increase in shear forces within the pDTA in patients who later developed ATBAD, accompanied by an elevated median OSI and RRT throughout the descending aorta. These observations indicate a potential association between changes in hemodynamic parameters in the descending aorta and the occurrence of ATBAD. This work sets the stage for computational modeling studies that test how we may influence these hemodynamic parameters at the index operation. Ultimately, the goal is that these insights can lead to more informed decision-making during aortic root surgery for patients with MFS, thereby reducing the occurrence of future

ATBAD and minimizing the need for readmissions or additional interventions.

Webcast

You can watch a Webcast of this AATS meeting presentation by going to: https://www.aats.org/resources/type-b-aortic-dissection-in-ma-6998.

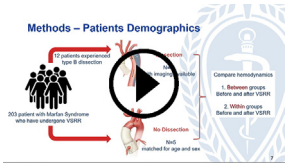

Conflict of Interest Statement

The authors reported no conflicts of interest.

The *Journal* policy requires editors and reviewers to disclose conflicts of interest and to decline handling or reviewing manuscripts for which they may have a conflict of interest. The editors and reviewers of this article have no conflicts of interest.

References

1. Milewicz DM, Dietz HC, Miller DC. Treatment of aortic disease in patients with Marfan syndrome. *Circulation*. 2005;111:e150-e157.
2. David TE, Feindel CM. An aortic valve-sparing operation for patients with aortic incompetence and aneurysm of the ascending aorta. *J Thorac Cardiovasc Surg*. 1992;103:617-622.
3. David TE, Park J, Tatangelo M, Steve Fan C-P, Ouzounian M. Cardiovascular events after aortic root repair in patients with Marfan syndrome. *J Am Coll Cardiol*. 2023;82:1068-1076.
4. Yildiz M, Nucera M, Jungi S, et al. Outcome of Stanford type B dissection in patients with Marfan syndrome. *Eur J Cardiothorac Surg*. 2023;64:ezad178.
5. Sulejmani F, Pokutta-Paskaleva A, Ziganshin B, et al. Biomechanical properties of the thoracic aorta in Marfan patients. *Ann Cardiothorac Surg*. 2017;6:610.
6. Wang Q, Guo X, Stäb D, et al. Computational fluid dynamic simulations informed by CT and 4D flow MRI for post-surgery aortic dissection–A case study. *Int J Heat Fluid Flow*. 2022;96:108986.
7. Camarda JA, Dholakia RJ, Wang H, Samyn MM, Cava JR, LaDisa JF Jr. A pilot study characterizing flow patterns in the thoracic aorta of patients with connective tissue disease: comparison to age-and gender-matched controls via fluid structure interaction. *Front Pediatr*. 2022;10:772142.
8. Guala A, Teixido-Tura G, Dux-Santoy L, et al. Decreased rotational flow and circumferential wall shear stress as early markers of descending aorta dilation in Marfan syndrome: a 4D flow CMR study. *J Cardiovasc Magn Res*. 2019;21:63.
9. van Der Palen RL, Barker AJ, Bollache E, et al. Altered aortic 3D hemodynamics and geometry in pediatric Marfan syndrome patients. *J Cardiovasc Magn Res*. 2016;19:30.
10. Bakhshinejad A, Baghaie A, Vali A, Saloner D, Rayz VL, D'Souza RM. Merging computational fluid dynamics and 4D Flow MRI using proper orthogonal decomposition and ridge regression. *J Biomech*. 2017;58:162-173.
11. McClarty D, Ouzounian M, Tang M, et al. Ascending aortic aneurysm haemodynamics are associated with aortic wall biomechanical properties. *Eur J Cardiothorac Surg*. 2022;61:367-375.
12. Nannini G, Caimi A, Palumbo MC, et al. Aortic hemodynamics assessment prior and after valve sparing reconstruction: a patient-specific 4D flow-based FSI model. *Comput Biol Med*. 2021;135:104581.
13. Tajeddini F, Romero DA, McClarty D, Chung J, Amon CH. Workflow comparison for combined 4D MRI/CFD patient-specific cardiovascular flow simulations of the thoracic aorta. *J Fluid Eng*. 2023;145:061106.
14. Tajeddini F, Romero Torres DA, McClarty D, Chung J, Amon CH. Combining 4D MRI with CFD for investigating patient-specific cardiovascular flows: a comprehensive comparison of ANSYS, COMSOL, and SimVascular illustrated with the prediction of thoracic aortic hemodynamics. Paper/Poster presented at: Fluids Engineering Division Summer Meeting, Toronto, Ontario, Canada, August 3, 2022.
15. Yushkevich PA, Piven J, Hazlett HC, et al. User-guided 3D active contour segmentation of anatomical structures: significantly improved efficiency and reliability. *Neuroimage*. 2006;31:1116-1128.
16. Saitta S, Maga L, Armour C, et al. Data-driven generation of 4D velocity profiles in the aneurysmal ascending aorta. *Comput Methods Programs Biomed*. 2023;233:107468.
17. Yu C-Y, Lin C-H, Yang Y-H. Human body surface area database and estimation formula. *Burns*. 2010;36:616-629.
18. Patel N, Durland J, Awosika AO, Makaryus AN. Physiology, Cardiac Index. In: StatPearls [Internet]. StatPearls Publishing; 2024.
19. Pirola S, Cheng Z, Jarral O, et al. On the choice of outlet boundary conditions for patient-specific analysis of aortic flow using computational fluid dynamics. *J Biomech*. 2017;60:15-21.
20. Armour CH, Guo B, Pirola S, et al. The influence of inlet velocity profile on predicted flow in type B aortic dissection. *Biomech Model Mechanobiol*. 2021;20:481-490.
21. Durbak E, Tarraf S, Gillespie C, et al. Ex vivo biaxial load testing analysis of aortic biomechanics demonstrates variation in elastic energy distribution across the aortic zone zero. *J Thorac Cardiovasc Surg*. 2023;166:701-712.e7.
22. Geiger J, Markl M, Herzer L, et al. Aortic flow patterns in patients with Marfan syndrome assessed by flow-sensitive four-dimensional MRI. *J Magn Reson Imaging*. 2012;35:594-600.
23. Hope TA, Kvitting J-PE, Hope MD, Miller DC, Markl M, Herfkens RJ. Evaluation of Marfan patients status post valve-sparing aortic root replacement with 4D flow. *Magn Reson Imaging*. 2013;31:1479-1484.
24. Geiger J, Hirtler D, Gottfried K, et al. Longitudinal evaluation of aortic hemodynamics in Marfan syndrome: new insights from a 4D flow cardiovascular magnetic resonance multi-year follow-up study. *J Cardiovasc Magn Reson*. 2016;19:33.
25. Matsuzawa Y, Lerman A. Endothelial dysfunction and coronary artery disease: assessment, prognosis, and treatment. *Coron Artery Dis*. 2014;25:713-724.
26. Tajeddini F, Nikmaneshi MR, Firoozabadi B, Pakravan HA, Ahmadi Tafti SH, Afshin H. High precision invasive FFR, low-cost invasive iFR, or non-invasive CFR?: optimum assessment of coronary artery stenosis based on the patient-specific computational models. *Int J Numer Method Biomed Eng*. 2020;36:e3382.
27. Allaire E, Hasenstab D, Kenagy RD, Starcher B, Clowes MM, Clowes AW. Prevention of aneurysm development and rupture by local overexpression of plasminogen activator inhibitor-1. *Circulation*. 1998;98:249-255.
28. Wanhainen A, Nilsson TK, Bergqvist D, Boman K, Björck M. Elevated tissue plasminogen activator in patients with screening-detected abdominal aortic aneurysm. *J Vasc Surg*. 2007;45:1109-1113.
29. Jana S, Hu M, Shen M, Kassiri Z. Extracellular matrix, regional heterogeneity of the aorta, and aortic aneurysm. *Exp Mol Med*. 2019;51:1-15.
30. Williams JG, Marlevi D, Bruse JL, et al. Aortic dissection is determined by specific shape and hemodynamic interactions. *Ann Biomed Eng*. 2022;50:1771-1786.
31. Louvelle L, Doyle M, Van Arsdell G, Amon C. The effect of geometric and hemodynamic parameters on blood flow efficiency in repaired tetralogy of Fallot patients. *Ann Biomed Eng*. 2021;49:2297-2310.
32. Schäfer M, Browne LP, Truong U, et al. Aortic stiffness in adolescent Turner and Marfan syndrome patients. *Eur J Cardiothoracic Surg*. 2018;54:926-932.
33. Youssefi P, Gomez A, He T, et al. Patient-specific computational fluid dynamics—assessment of aortic hemodynamics in a spectrum of aortic valve pathologies. *J Thorac Cardiovasc Surg*. 2017;153:8-20.e3.
34. Yoshida S, Toda K, Miyagawa S, Sawa Y. Computational fluid dynamics visualizes turbulent flow in the aortic root of a patient under continuous-flow left ventricular assist device support. *J Thorac Cardiovasc Surg*. 2020;159:e205-e207.

Key Words: acute type B aortic dissection, computational fluid dynamics, David procedure, hemodynamics, Marfan syndrome, valve-sparing root replacement

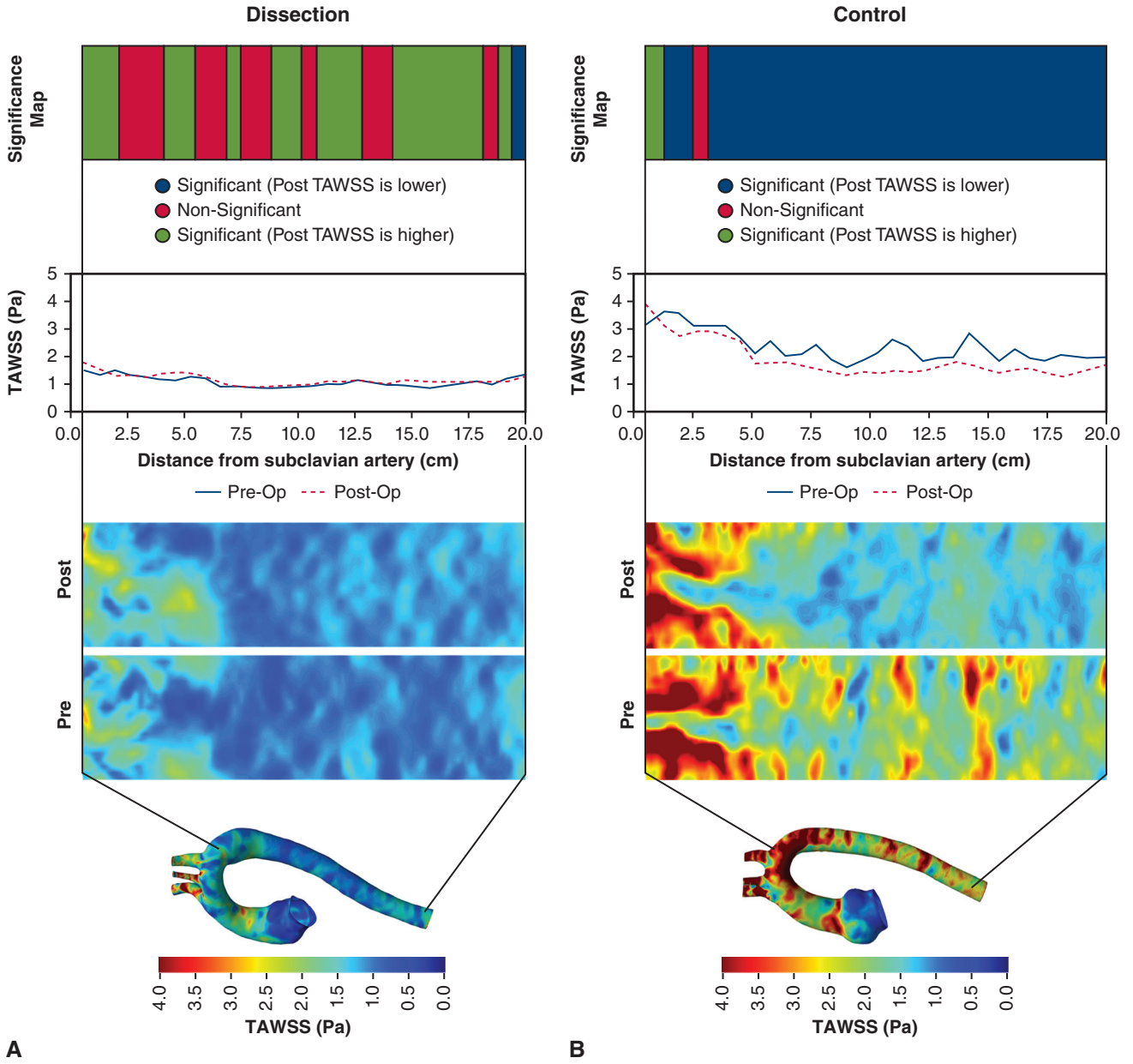

FIGURE E1. Comprehensive analysis for pair 2, comprising a preoperative 3-dimensional contour of TAWSS on the thoracic aorta, preoperative and postoperative 2-dimensional maps of TAWSS, a curve illustrating the preoperative and postoperative medians over different segments of the descending aorta, and a map displaying the *t* test results for differences in postoperative and preoperative TAWSS for each segment. In the *t* test map, red indicates a significant increase in TAWSS after the operation, blue indicates a significant decrease, and gray denotes no significant difference in pre and postoperative TAWSS. Also, each segment represents a 5-mm interval. *TAWSS*, Time-averaged wall shear stress.

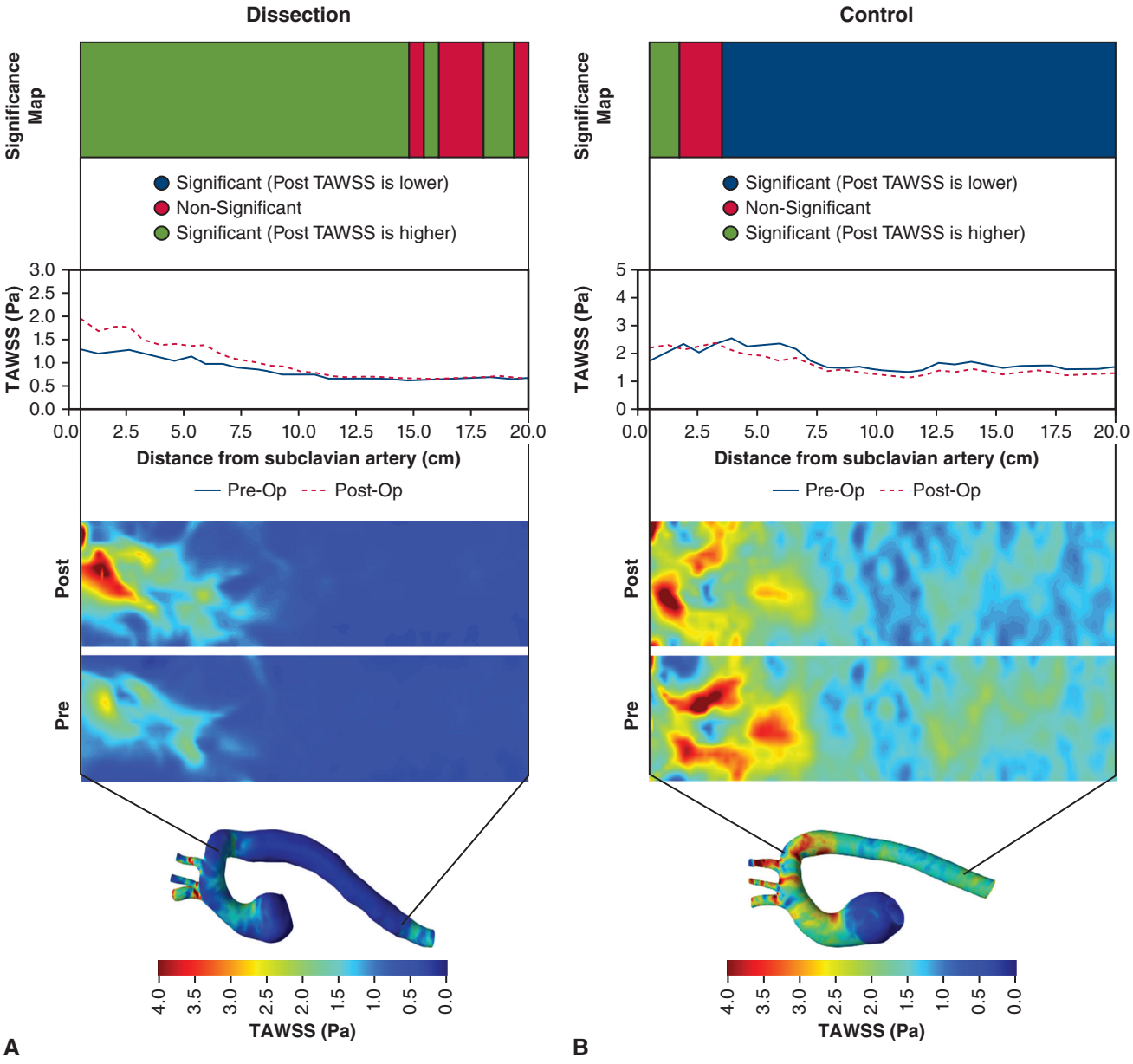

FIGURE E2. Comprehensive analysis for pair 3, comprising a preoperative 3-dimensional contour of TAWSS on the thoracic aorta, preoperative and postoperative 2-dimensional maps of TAWSS, a curve illustrating the preoperative and postoperative medians over different segments of the descending aorta, and a map displaying the *t* test results for differences in postoperative and preoperative TAWSS for each segment. In the *t* test map, *green* indicates a significant increase in TAWSS after the operation, *blue* indicates a significant decrease, and *red* denotes no significant difference in preoperative and postoperative TAWSS. Also, each segment represents a 5-mm interval. *TAWSS*, Time-averaged wall shear stress.

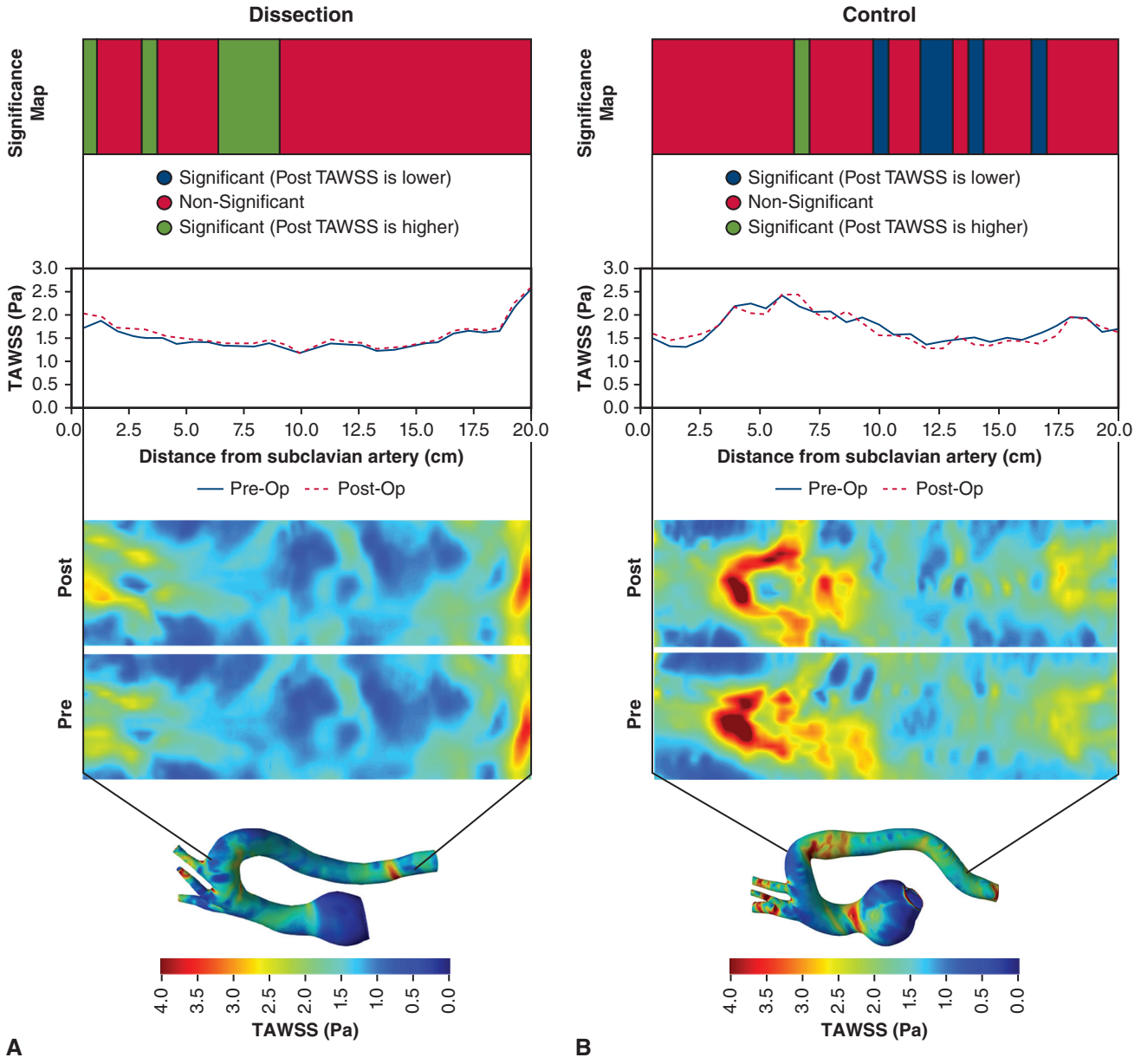

FIGURE E3. Comprehensive analysis for pair 4, comprising a preoperative 3-dimensional contour of TAWSS on the thoracic aorta, preoperative and postoperative 2-dimensional maps of TAWSS, a curve illustrating the preoperative and postoperative medians over different segments of the descending aorta, and a map displaying the *t* test results for differences in postoperative and preoperative TAWSS for each segment. In the *t* test map, *green* indicates a significant increase in TAWSS after the operation, *blue* indicates a significant decrease, and *red* denotes no significant difference in preoperative and postoperative TAWSS. Also, each segment represents a 5-mm interval. *TAWSS*, Time-averaged wall shear stress.

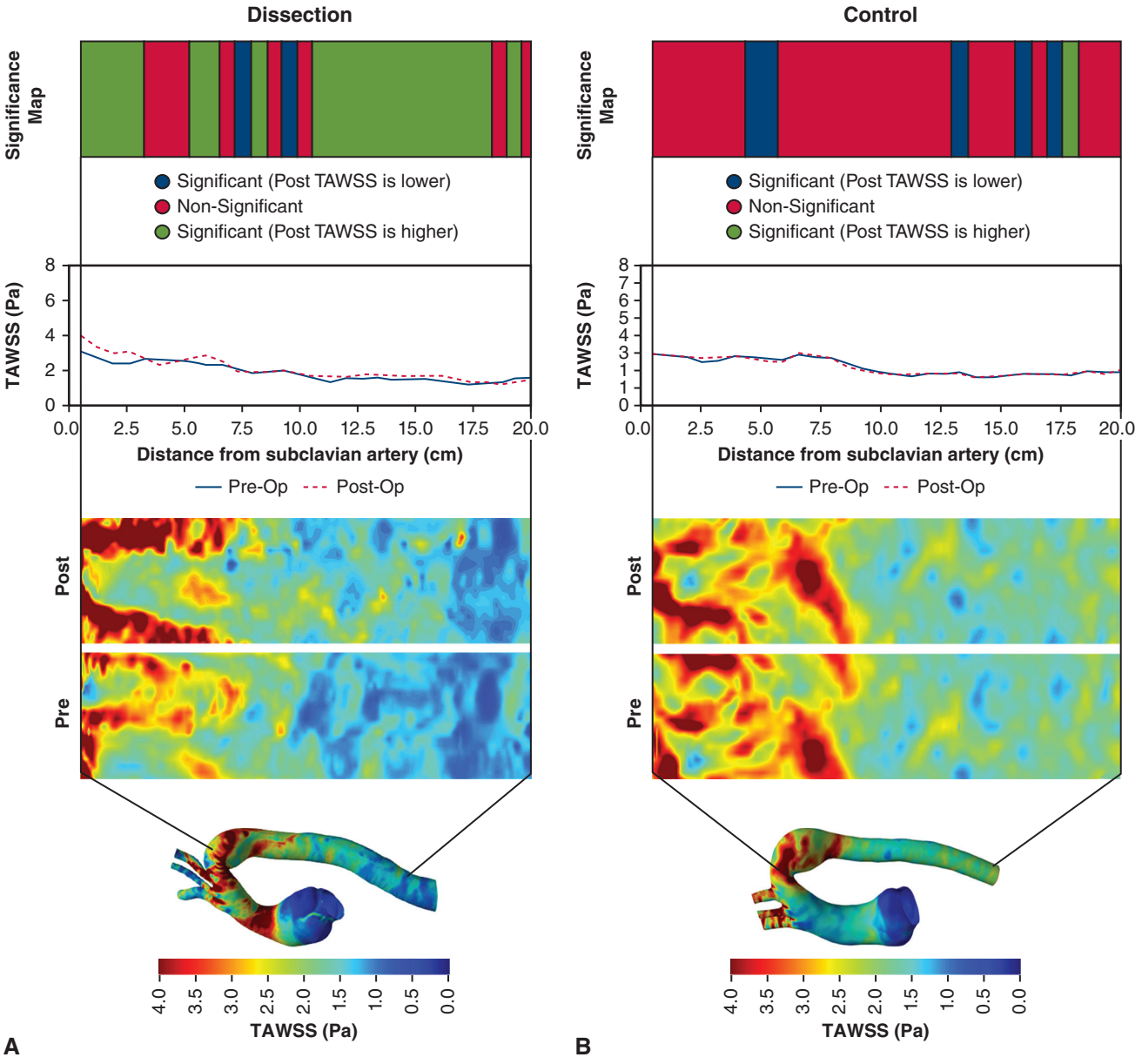

FIGURE E4. Comprehensive analysis for pair 5, comprising a preoperative 3-dimensional contour of TAWSS on the thoracic aorta, preoperative and postoperative 2-dimensional maps of TAWSS, a curve illustrating the preoperative and postoperative medians over different segments of the descending aorta, and a map displaying the *t* test results for differences in postoperative and preoperative TAWSS for each segment. In the *t* test map, *green* indicates a significant increase in TAWSS after the operation, *blue* indicates a significant decrease, and *red* denotes no significant difference in preoperative and postoperative TAWSS. Also, each segment represents a 5-mm interval. *TAWSS*, Time-averaged wall shear stress.